Dispersion of ferrofluid aggregates in steady flows

Alicia M. Williams and Pavlos P. Vlachos

Citation: Physics of Fluids (1994-present) **23**, 127102 (2011); doi: 10.1063/1.3670012
View online: http://dx.doi.org/10.1063/1.3670012
View Table of Contents: http://scitation.aip.org/content/aip/journal/pof2/23/12?ver=pdfcov
Published by the AIP Publishing

Dispersion of ferrofluid aggregates in steady flows

Alicia M. Williams[1] and Pavlos P. Vlachos[2]
[1]*Lawrence Livermore National Laboratory, Livermore, California 94550, USA*
[2]*Mechanical Engineering Department, Virginia Polytechnic Institute and State University, Blacksburg, Virginia 24061, USA*

(Received 8 April 2011; accepted 7 November 2011; published online 14 December 2011)

Using focused shadowgraphs, we investigate steady flows of a magnetically non-susceptible fluid interacting with ferrofluid aggregates comprised of superparamagnetic nanoparticles. The ferrofluid aggregate is retained at a specific site within the flow channel using two different applied magnetic fields. The bulk flow induces shear stresses on the aggregate, which give rise to the development of interfacial disturbances, leading to Kelvin-Helmholtz (K-H) instabilities and shedding of ferrofluid structures. Herein, the effects of bulk Reynolds number, ranging from 100 to 1000, and maximum applied magnetic fields of 1.2×10^5 and 2.4×10^5 A/m are investigated in the context of their impact on dispersion or removal of material from the core aggregate. The aggregate interaction with steady bulk flow reveals three regimes of aggregate dynamics over the span of Reynolds numbers studied: stable, transitional, and shedding. The first regime is characterized by slight aggregate stretching for low Reynolds numbers, with full aggregate retention. As the Reynolds number increases, the aggregate is in-transition between stable and shedding states. This second regime is characterized by significant initial stretching that gives way to small amplitude Kelvin-Helmholtz waves. Higher Reynolds numbers result in ferrofluid shedding, with Strouhal numbers initially between 0.2 and 0.3, wherein large vortical structures are shed from the main aggregate accompanied by precipitous decay of the accumulated ferrofluid aggregate. These behaviors are apparent for both magnetic field strengths, although the transitional Reynolds numbers are different between the cases, as are the characteristic shedding frequencies relative to the same Reynolds number. In the final step of this study, relevant parameters were extracted from the time series dispersion data to comprehensively quantify aggregate mechanics. The aggregate half-life is found to decrease as a function of the Reynolds number following a power law curve and can be scaled for different magnetic fields using the magnetic induction at the inner wall of the vessel. In addition, the decay rate of the ferrofluid is shown to be proportional to the wall shear rate. Finally, a dimensionless parameter, which scales the inertia-driven flow pressures, relative to the applied magnetic pressures, reveals a power law decay relationship with respect to the incident bulk flow. © *2011 American Institute of Physics*. [doi:10.1063/1.3670012]

I. INTRODUCTION

Ferrofluids are stable suspensions of subdomain particles that become strongly magnetized in the presence of a magnetic field. The interaction of ferrofluids with magnetic fields adds a dimension of physics beyond those of conventional fluid mechanics and is the basis of the field of ferrohydrodynamics. Studies of ferrofluids include those focusing on the apparent change in viscosity of a ferrofluid under a magnetic field[1] or on the behavior of these magnetically susceptible fluids due to changes in magnetic field strength.[2] Moreover, fluid instabilities have been the subject of significant scientific works, including the spike-shaped protrusions from a ferrofluid free surface known as the normal field instability,[3,4] the labyrinthine instability,[5] and the Rayleigh-Taylor instability.[6] The Kelvin-Helmholtz instability in ferrofluids has also been studied in several papers analytically,[7–9] but has been largely neglected experimentally.

Ferrofluids have been at the center of many new inventions since the advent of ferrofluid research in the 1960s, including improved dampers and seals.[10] Some of the newest ferrofluid applications have been focused on their integration in a new technique for targeting disease treatment in the human body.[11–15] Magnetic drug targeting (MDT) involves magnetically guiding droplets of a biocompatible ferrofluid bonded reversibly to specific chemotherapeutic agents, which are injected into the blood or lymphatic circulation system.[15] Some trials performed on lab animals have shown that 50% of the typical systemic dose applied to treat cancerous tumors can result in remission of the tumor after only one treatment of anticancer drugs with MDT.[11,15–17] Though these studies have provided proof that the MDT application has promise as a clinical modality, only a few physics-based works have examined the interaction of the ferrofluid aggregate with an incident non-magnetic flow. Understanding the governing physics and scaling of the ferrofluid dispersion and retention could aid in the development of improved MDT methodologies.

Initial experimental contributions towards understanding ferrofluid-fluid interactions were published by Ruuge and Rusetski[18,19] as well as Ganguly *et al.*[20–22] In the work of Ruuge and Rusetski, an aggregate of ferrofluid was

accumulated in a tube prior to the startup of bulk flow. Ferrofluid dispersion was measured using gamma-active tagging over a wide range of flows, and the authors examined the long-time dispersion of the ferrofluid. In Ganguly's work, shadowgraphs were used as a means to analyze the behavior of ferrofluid aggregates as ferrofluid is injected into a test section. One of the primary results from these initial studies is the periodic buildup and shedding of a ferrofluid aggregate accumulated by a permanent magnet at Reynolds numbers below 400 observed over several minutes of data acquisition. The results of these works will be discussed in further detail in the context of the results obtained from present experimentation.

Herein, we extend upon previous works by examining the interaction of a ferrofluid aggregate with a non-magnetic fluid under steady flows for bulk flow Reynolds numbers (Re) ranging between 100 and 1000 and under the action of two separate applied magnetic fields. In order to extract the dynamics of the flow-ferrofluid interaction, measurements are performed using focused shadowgraphs and the recorded images are quantitatively analyzed using digital image processing. Under the action of the magnetic field, the aggregate behaves similarly to a bluff-body, inducing shear-layers and generating a wake as well as vortex shedding. However, since the aggregate bluff-body is essentially comprised of a fluid, it deforms dynamically and according to the shear and normal stresses induced by the bulk flow and the magnetic field. The result is reduction in size of the body as the induced forces cause the ferrofluid to break up and disperse downstream, in the direction of the bulk flow.

This paper will first present the experimental method for recording focused shadowgraphs as well as the algorithms for quantitatively post-processing the raw frames. The aggregate dynamics will be presented in terms of the evolution of the aggregate size and shedding frequency over time as functions of both the magnetic field and Reynolds number. Finally, single parameters, including a dimensionless parameter, are used to delineate aggregate behavior and are presented as a means to capture the aggregate physics observed across the identified regimes.

II. EXPERIMENTAL METHODS

For the experiment presented here, ferrofluid is introduced and is allowed to interact with a steady flow in a square channel with hydraulic diameter $D_h = 0.015$ m. A square channel was selected over a circular channel to avoid introducing additional three-dimensional effects to the dynamics of the aggregate, focusing on the basic aggregate physics. The Reynolds numbers based on the bulk flow parameters (average velocity U_o, hydraulic diameter D_h, density of water ρ, dynamic viscosity of water μ, and kinematic viscosity of water ν) ranged between 100 and 1000. In addition, two magnetic fields with values of 1.2 and 2.4×10^5 A/m were considered in order to allow for investigating the scaling of the magnetic forces. The experimental test matrix is provided in Table I. For the second (higher) magnetic field, Reynolds numbers of 700 and 800 were later deemed unusable and were not further analyzed.

TABLE I. Experimental test matrix to study aggregate dispersion.

Applied magnetic field, A/m	Reynolds numbers investigated
1.2×10^5	100 to 1000 in steps of 100
2.4×10^5	100 to 600 in steps of 100, 900, and 1000

The data were obtained using focused shadowgraphs, which are particularly effective when investigating phenomena that involve fluids with distinct density gradients or an opacity differential that generates a high contrast interface, as is the case of ferrofluid and water studied herein. Illumination for the shadowgraph background was provided by a 250 Watt halogen white light source that was directed through spherical and ground glass lenses to illuminate a region of interest with uniform intensity of 2 by 15 cm in size. The lighting was directed at the square channel, illuminating the region in which the ferrofluid was retained. A schematic depicting the setup for the shadowgraph experiments is shown in Figure 1.

A digital charge-coupled device (CCD) camera sampling at 50 Hz was used to image the side plane of the test section where the ferrofluid aggregate was retained. A total of 3000 images were acquired for each case, corresponding to a recording time of 60 s. The image magnification was 63 microns/pixel with an image size of 1020 by 500 pixels. This interrogation region encompassed the channel height as well as 4 D_h in the streamwise direction. This experiment compares differently to those of Ganguly *et al*. in that the focus was placed on the acute transient behavior of the aggregate and its interfacial dynamics, whereas previous works focused on long-term residence time of ferrofluid aggregates at lower Re.

In each case, a 2 ml volume of water-based ferrofluid (EMG 705, Ferrotec, Inc.) was injected 4 D_h upstream of the

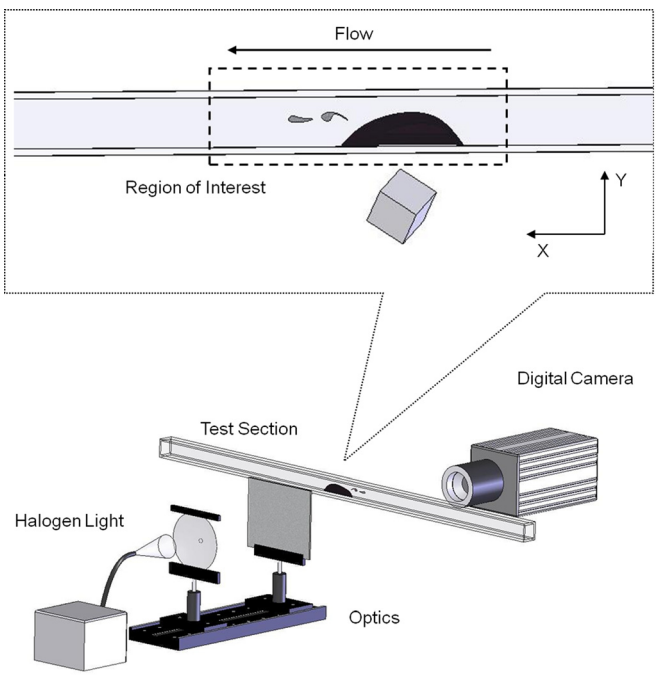

FIG. 1. (Color online) Schematic of focused shadowgraph experiment. A high-speed digital camera imaged the side profile of the ferrofluid aggregate.

region of interest before each test in quiescent conditions at a rate of 1 ml per min. EMG 705 ferrofluid has a saturation magnetization of 22 mT, a nominal density of 1.19 g/cc, and a nominal magnetic particle concentration of 3.9% by volume, with a mean particle diameter of 10 nm. The ferrofluid was diluted to 2% of its original concentration by mixing with water. Injection was facilitated by a needle aligned parallel to the test section walls and mounted flush to the bottom wall of the channel. A KD Scientific 230 syringe pump was utilized for all injection, with an estimated accuracy of 1% full-scale volumetric flow. The ferrofluid was captured and retained by a 0.5 Tesla permanent magnet that was obliquely oriented with one of its vertices closest to the test section, resulting in a maximum magnetic field of 1.2×10^5 and 2.4×10^5 A/m at the inner test section wall. The magnetic field was varied by means of a micro-positioning traverse.

The bulk flow (water) was switched on after the ferrofluid was accumulated and settled, flowing in the positive x-direction. The flow rate was measured using a Transonic Systems T110 ultrasonic flow meter with an absolute accuracy of 10%. The test section was 1 meter in length to enable fully developed flow for all Reynolds numbers examined in this work relative to the quiescent flow aggregate height of 7 mm. Flow was ramped up over 0.1 s, which ensured quasi-steady acceleration for all cases based on the inertial time scale υ/U_o^2. It should be noted that the aggregate formation and subsequent interactions are only dependent on the presence of the magnetic field. When the magnet is removed, the aggregate disperses instantaneously in the positive x-direction as the ferrofluid is superparamagnetic, and does not retain its magnetism in the absence of a magnetic field.

The magnetic field was characterized using a DC Gaussmeter (Alphalab, Inc., 1 Gauss resolution at 20 000 Gauss dynamic range). The applied magnetic field is primarily two-dimensional, due to the oblique orientation of the magnet. The oblique orientation also provides high magnetic field gradients, with the primary direction of the field being perpendicular to the direction of bulk flow. Contours of the spatial distribution of the resulting normal magnetic induction are shown in Figure 2, with out-of-plane magnetic induction neglected in subsequent analysis. This distribution is used to estimate the magnetic field strength at the corresponding ferrofluid-fluid interface heights for analysis presented in proceeding sections. Alterations of the magnetic field due to the presence of the magnetized ferrofluid were not considered in this work. The applied magnetic field is calculated from the measured magnetic induction using the formula

$$H = \frac{B}{\mu_0}, \tag{1}$$

where μ_o is the permeability in a vacuum ($4\pi \times 10^{-7}$ N/A^2) and B is the magnetic field induction. In this work, the maximum value of H, or H_{max}, is used to denote the value of the maximum magnetic field at the location of the inside wall the flow channel.

The raw frames obtained by the focused shadowgraph technique were post-processed to determine the aggregate size evolution in time as well as to detect the shedding

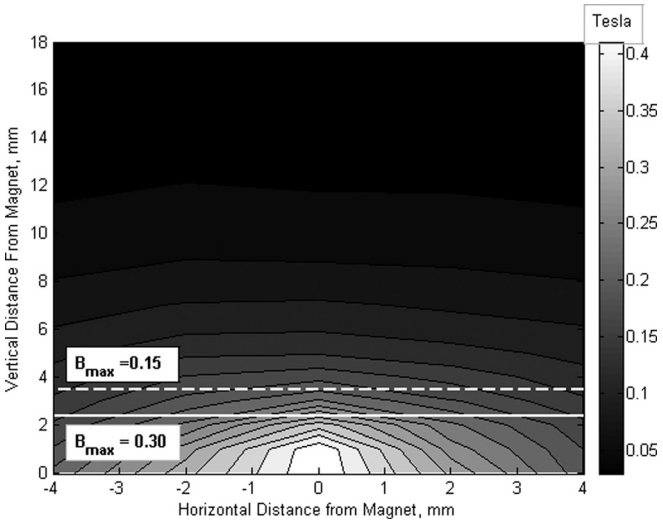

FIG. 2. Contours of magnetic field induction in the z-direction (Tesla). The highest field gradients are near the magnet tip at (x, y) = (0, 0). The magnetic field is shown relative to the channel bottom for both maximum magnetic fields of 0.30 and 0.15 Tesla.

frequency of the Kelvin-Helmholtz rolls shed from the aggregate. First, the methodology used to extract the aggregate size in time will be discussed, and then, a separate process used to determine the shedding frequency over time will be presented.

Figure 3 shows the steps taken to measure the evolving size of the aggregate over time. The interface between the ferrofluid and water was sampled for each snapshot of the flow using software written in-house in conjunction with the MATLAB image processing toolbox. The grayscale images were converted to black and white using Otsu's[23] grayscale thresholding algorithm. Otsu's method assumes uniform image illumination and a bimodal image histogram, used as a basis to binarize each image. Regions of connected pixels in the binary images were identified and sorted by size for each frame, which represent the ferrofluid aggregate or vortex shedding. The size of the aggregate was obtained using this method by selecting the largest region, which was confirmed through the output of the binarized image. The aggregate size, measured from the binary images, was corrected

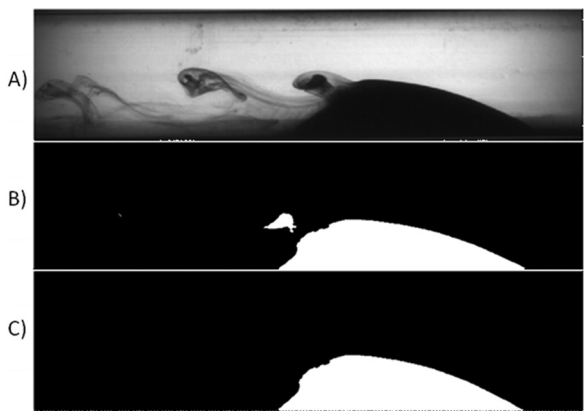

FIG. 3. The image processing used to transform a grayscale raw image (a) to a binary image (b) to an image in which the instantaneous aggregate was isolated (c).

by weighting with the grayscale intensity of the pixels in the region of the aggregate. The intensities account for the local ferrofluid concentration and correct the aggregate size by up to 10%. Pixel intensities are a factor when calculating the time-rate of dispersion, particularly as the aggregate deforms in the x and y-directions. Image binarization was performed based on the intensity distribution of each individual image, and, therefore, does not account for bulk flow-driven reductions in the local ferrofluid concentration. The variation in initial aggregate size was estimated to 5% across all cases. In addition, the random error in the aggregate size measurement is estimated to be +/−0.5%, based on the measured variance between two successive frames of a ferrofluid aggregate retained in quiescent flow.

In the case in which the aggregate disperses through the unsteady shedding of vortices, it was desired to measure the shedding frequency over the data acquisition time. Similarly to the method used to isolate the aggregate size, the images were binarized, focusing on the region just downstream of the aggregate. Figure 4 shows a sample image with the region of interrogation, which is subdivided into five smaller windows for the binarization that have 15 pixel width by 200 pixel height. Tall windows spanning the majority of the channel height are required to consistently capture the shed ferrofluid as the height of the aggregate changes significantly over time in the case of K-H shedding. The fraction of black pixels relative to the total number of pixels per window was recorded for each of the five windows over time, and then the average fraction from the individual windows was calculated for each frame, corresponding to a single time instant.

The measured fraction of dark pixels with respect to the total number of pixels in the window is shown in Figure 5 for a sample case with a bulk Reynolds number of 500 and magnetic field of $H_{max} = 1.2 \times 10^5$. The time series is detrended for processing as shown in Figure 5(b). After detrending, the signal remains nonstationary and nonergodic, and, therefore, for the spectral analysis, we used short time Fourier transform (STFT).[24,25] A sample STFT corresponding to the data from Figure 5 is shown in Figure 6, where 512 point Hanning windows were used in conjunction with a 75% overlap for a frequency resolution of 0.1 Hz. The shedding frequencies were extracted from each band in the STFT by determining the frequency corresponding to the peak value from the STFT corresponding to each time band as in Figure 7. These shedding frequencies were confirmed by manually estimating the shedding frequency using the raw frames. This provides information complementary to the aggregate dispersion measurements in that the shedding frequencies indicate rates of aggregate decay.

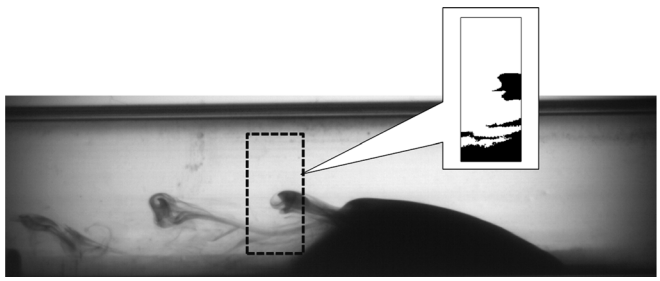

FIG. 4. Binarization of ferrofluid shed from aggregate to determine shedding frequency.

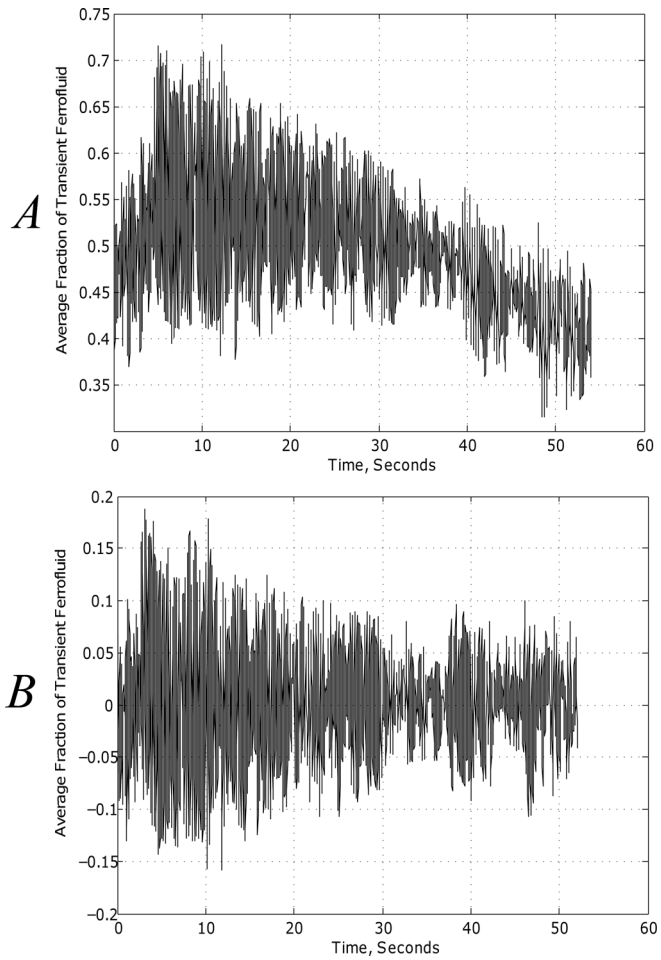

FIG. 5. (a) Sample time series of raw detected fraction of ferrofluid passing through image windows through time. (b) De-trended fraction of ferrofluid passing through image windows over time.

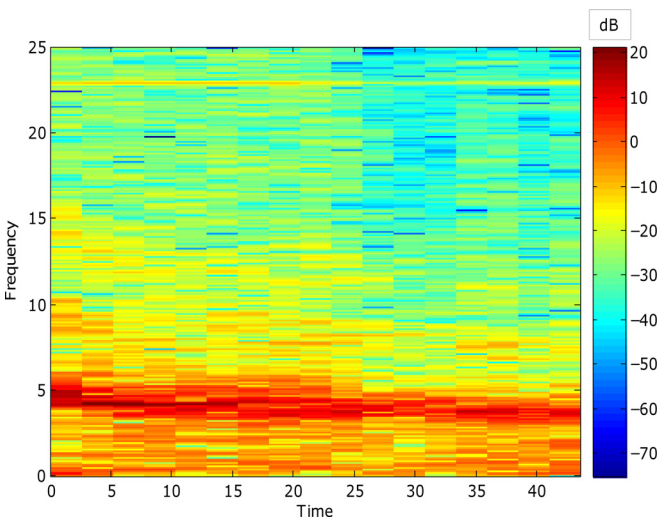

FIG. 6. (Color online) Sample short time Fourier transform for Re = 500 with $H_{max} = 1.2 \times 10^5$ A/m.

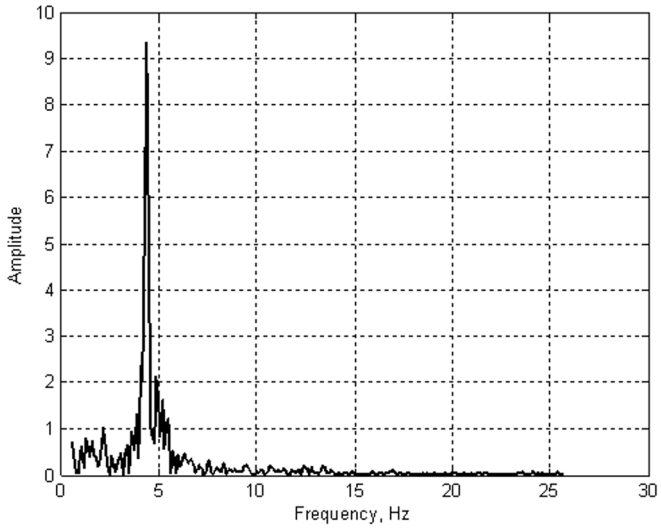

FIG. 7. Extraction of amplitude versus frequency during one time period extracted from the STFT in Figure 6. The peak energy corresponds to the shedding frequency of the aggregate.

III. RESULTS

A. Aggregate dispersion characteristics

The large-scale changes of the aggregate are characterized by three primary dispersion regimes: stable, transitional, and shedding. A representative set of shadowgraph images of cases with Reynolds numbers corresponding to the three regimes is shown in Figure 8. For Reynolds numbers below 400, slight aggregate stretching occurs in the positive x and y-directions, and the aggregate is displaced downstream. No measurable reduction in aggregate mass is observed in two dimensions as interrogated by side-oriented digital imaging in these cases. The aggregate is three-dimensional, however, during the largely static behavior of these low Re cases, aggregate dynamics are largely two-dimensional. For a Reynolds number of 400, stretching in the positive x and y-directions occurs initially, resulting in a slight apparent increase in aggregate size due the two-dimensional measurement method. The biaxial stretching ultimately overcomes the magnetic body forces, since the aggregate expands beyond regions of high magnetic field gradients wherein, it is controlled by the magnet. Stretching in the direction of the bulk flow leads to the growth of interfacial waves on the aggregate and slight wisps of ferrofluid are shed. As the Reynolds number is increased to 500 or greater, the aggregate centroid translates significantly in the positive x-direction when exposed to flow pressure, which also results in significant aggregate stretching along this axis. As a result of both the aggregate deformation and interfacial excitation, the Kelvin-Helmholtz instability develops and leads to shear layer shedding. As a result, the aggregate decays rapidly as ferrofluid vortices are shed, with three-dimensional structures apparent in the shadowgraph data.

The primary difference between the two field inductions becomes apparent at $\mathrm{Re} = 300$ as shown in Figure 9. The case with the lower magnetic field remains in the stable regime, while at H_{max} of 2.4×10^5, the aggregate destabilizes and washes away. As the Reynolds number increases past 400, the effect of the increased field is diminished in terms of observable differences in regime-based dynamics, as inertial effects dominate the aggregate characteristics. The fundamental mechanics of aggregate behavior are illustrated in Figure 10. Three time instants of the main aggregate outline are plotted for a Reynolds number of 500, H_{max} of 2.4×10^5, beginning with the primary ferrofluid-fluid boundary in quiescent conditions. As flow is ramped, the centroid of the aggregate translates in the positive x-direction, while the aggregate stretches out as flow is ramped. The aggregate then rebounds towards its starting location (centered over the magnet tip), which fosters interfacial perturbations and the initial appearance of the K-H instability.

For all Reynolds numbers, the relative size of the aggregate (a/a_i) is plotted versus time in Figure 11 for maximum fields of 1.2×10^5 and 2.4×10^5 A/m. The dispersion was calculated as the normalized sum of the number of pixels in the edge-detected aggregate with respect to the initial aggregate size, a_i. The normalization using the initial aggregate size provides the relative change in aggregate size over time. When the Reynolds number is lower than 400 with H_{max} of 1.2×10^5, an increase of the apparent aggregate size is manifested by a slightly upward sloping line, indicating aggregate stretching due to shear stresses. The stretching increases from 3.8 to 6.3, and finally, 8% for Reynolds numbers between 100 and 300. The initial aggregate stretching is similar when H_{max} is 2.4×10^5 for Reynolds numbers up to 300.

At the transition point of $\mathrm{Re} = 400$ with $H_{max} = 1.2 \times 10^5$ and $\mathrm{Re} = 300$ with $H_{max} = 2.4 \times 10^5$ A/m, a conspicuous

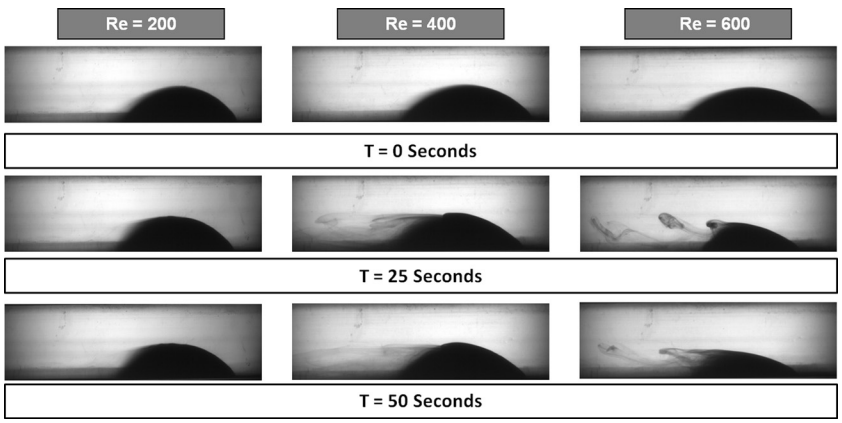

FIG. 8. Shadowgraph images for three time instants of 0, 25, and 50 s with Reynolds numbers of 200, 400, and 600. For a Reynolds number of 600, Kelvin-Helmholtz shedding occurs, causing the aggregate to wash away.

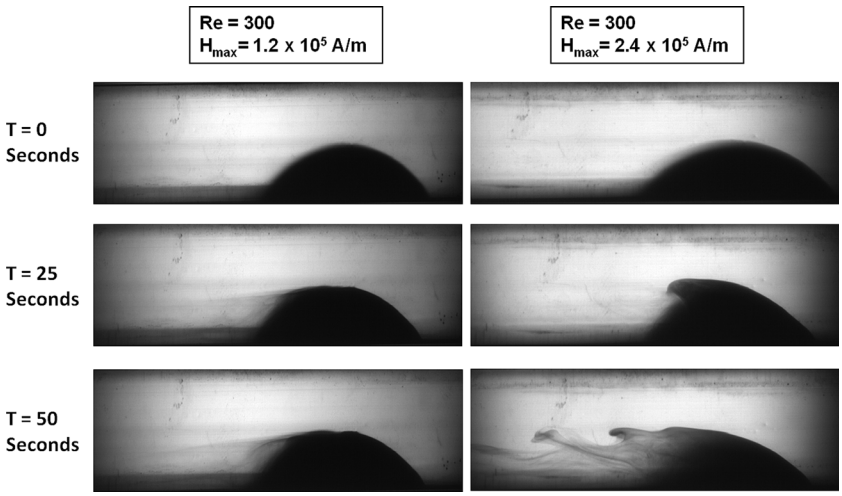

FIG. 9. The impact of magnetic field strength for magnetic fields of 1.2×10^5 and 2.4×10^5. For the stronger magnetic field, the aggregate destabilizes and K-H shedding occurs from the aggregate approximately 25 s after the start of flow.

increase in the aggregate size occurs initially, stretching up to 10% and 7%, respectively. After stretching, wisps of ferrofluid are periodically shed from the aggregate, and the aggregate begins to disperse. The incipient destabilization at transition for the higher magnetic field is more pronounced, and therefore, significant aggregate dispersion occurs, resulting in a size reduction of 14% of the initial aggregate. As the Reynolds number is increased past the transition point for both field strengths, the initial stretching of the aggregate occurs rapidly, within the first seconds after flow ramp-up. After the initial stretching, the aggregate destabilizes and decays exponentially through Kelvin-Helmholtz shedding.

The evolution of shedding of the aggregate is captured in Figure 12, where the Strouhal number (St) is plotted against the normalized specific volume-based magnetic body force, F_M, for the two applied magnetic fields. The Strouhal number is calculated based on the shedding frequency of the ferrofluid aggregates

$$St = \frac{f_s h}{U_b}, \tag{2}$$

where U_b represents the blockage velocity of the water flowing over the aggregate, which is a function of aggregate height. The parameter h represents the instantaneous aggregate height. f_s is the measured shedding frequency of the ferrofluid whorls in radians per second. The magnetic forces are captured by the specific volume-based magnetic body force, F_M

$$F_m = (M \bullet \Delta)H, \tag{3}$$

which is calculated using the magnetization of the ferrofluid, M (*Tesla*), and the spatially resolved applied magnetic field, H (*Amperes/meter*). The magnetization was determined using Langevin's equation, and body force was calculated at the interface between the ferrofluid aggregate and the bulk flow using the aggregate height extracted from the imaging data. A value for F_M in terms of force per unit volume was calculated at each time instance and is normalized to the magnetic body force measured at the start of each case, $F_{M,0}$. This normalization delineates how the aggregate size and body forces change relative to the Strouhal number plotted on the y-axis.

Shedding frequencies were measured from the raw frames as described in the methods section, with the first 5 s

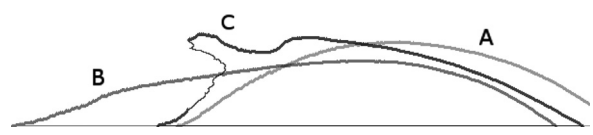

FIG. 10. Line plot illustrating transition of the aggregate into a K-H shedding regime. (a) Quiescent flow, t = 0 s, (b), aggregate stretching, t = 0.56 s, and (c) main aggregate outline during ferrofluid shedding, t = 9 s.

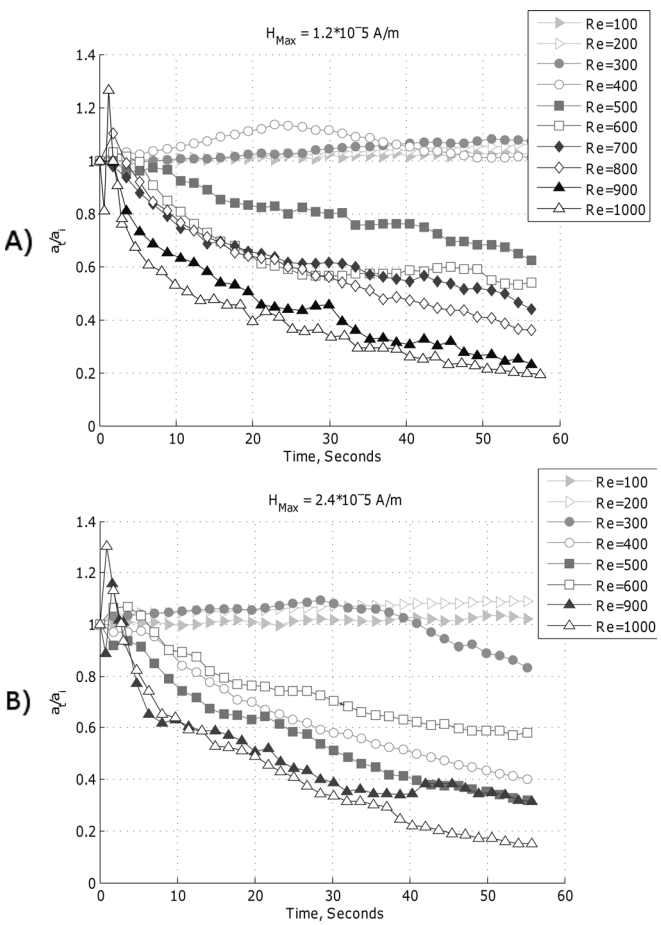

FIG. 11. Plots of the apparent aggregate size versus time with H_{max} of 1.2×10^5 and 2.4×10^5 A/m.

of data acquisition neglected since large plugs of ferrofluid initially slough off from the aggregate as flow is ramped up. Flow startup is distinguished from the startup of shedding, though this large perturbation of the aggregate appears to initiate K-H shedding. For post-processing purposes, the height of the aggregate was downsampled with 512 point subsets of the signal and averaged with 75% overlap, therefore, matching the temporal resolution of the shedding frequencies.

Many of the dynamics observed in the shadowgraphs are quantified in Figure 12. Application of a higher magnetic field results in higher shedding frequencies initially compared to lower magnetic fields. Moreover, the shedding frequencies are highest at the onset of shedding, when the aggregate is the largest and subjected to the greatest shear from the flow. The high shedding frequencies at the start of each case also drive the initial rapid drop in aggregate size, as shedding is the mechanism by which the aggregate disperses. From Figure 12, initial values of St start at approximately 0.2 and increase as Re increases. Roshko[26] and Williamson[27] reported St varying between approximately 0.16 and 0.21 for Re varying between 100 and 1000. Using these St to predict the initial shedding frequency based on the blockage velocity associated with the initial aggregate height after flow ramp up (transition to shedding), the calculated values range from 0.6 Hz for Re = 100 to 8 Hz for Re = 1000. These shedding frequencies are close to the measured values for cases where K-H shedding was observed, but also assume a fully rigid interface. Measured shedding frequencies (and resulting St) in Figure 12 are generally higher than the prediction, which is attributed to the dynamic interaction of the ferrofluid interface with the bulk flow. However, for low Re, no shedding was measured from the ferrofluid aggregate. In Figure 12, the normalized value of F_M is also analogous to time, since the magnetic body forces at the aggregate-flow interface increase as the aggregate washes away. As wash away occurs, the aggregate height reduction acts to reduce the shedding frequency due to decreased shear stresses from the incident flow. Conversely, the magnetic body forces are increasing and assist in aggregate retention, further resisting shedding.

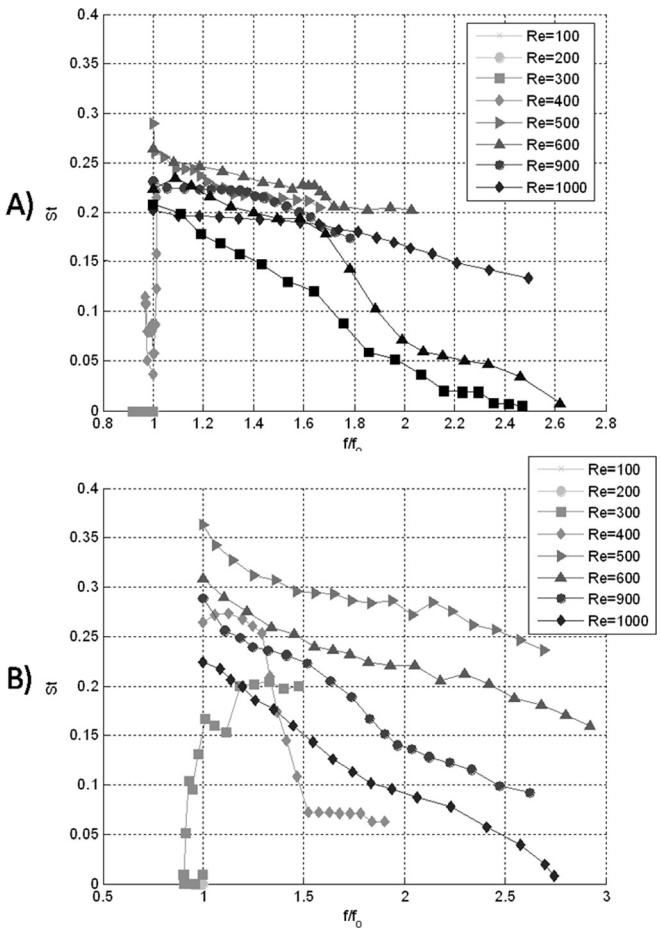

FIG. 12. Strouhal number versus normalized magnetic body forces for (a) H_{max} of 1.2×10^5 and (b) H_{max} of 2.4×10^5 A/m. Low Re cases have values of f/f_o near 1 and have a continuously zero value of St due to lack of shedding phenomena.

Unlike cases with significant dispersion, low Reynolds numbers that do not exhibit any shedding behavior have zero-valued St in Figure 12, with relatively stable values of $F_M/F_{M,0}$. On the other hand, cases that are transitioning to shedding have increasing Strouhal numbers over time, and very slight amounts of aggregate decay. These aggregates increase in height in the y-direction initially due to stretching, and then decrease as the aggregate begins to disperse. The height decrease occurs as the shedding frequency increases and ferrofluid advects away from the aggregate. Cases with large amounts of shedding have magnetic body forces that increase consistently over time. For transitional cases, this data set captures only the increase in St as the aggregate initially transitions into a shedding mode. If additional temporal data were available, we would anticipate that the St will eventually begin to decrease as the aggregate height drops subsequent to ferrofluid vortex shedding, following curves similar to those shown at moderate Reynolds numbers.

Additional insight into the relationship between aggregate shedding and aggregate size is provided by examining the aspect ratio of the aggregate. Figure 13 shows the aspect ratio measured at the ferrofluid aggregate half-life, as defined by the aggregate length divided by twice the aggregate height. Consistent increases in the aspect ratio occur as a

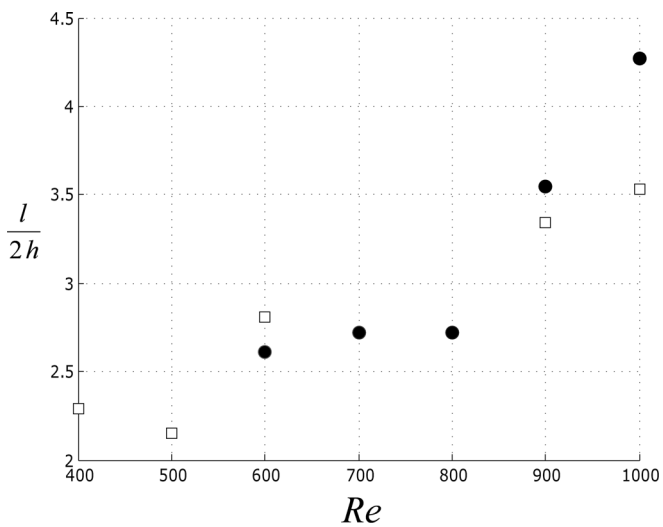

FIG. 13. Plot of the aspect ratio calculated at the time corresponding to the aggregate half-life as a function of Reynolds number.

function of Reynolds number, indicating relative aggregate lengthening in the streamwise direction due to flow shearing. Independently, examining the aggregate length, a slight decay occurs as a function of Re. However, the height of the aggregate at the half life reduces by a factor of approximately three between low Re and high Re. The aspect ratio data is also useful for relating to generalized fluid mechanics studies, which provide additional data revealing the interaction between the ferrofluid aggregate and bulk flow. In an analytical study of compliant bodies subjected to moderate cross-flows, Yokoyama and Mochizuki[28] found that lower stiffness compliant cylinders subjected to cross flows deform and elongate into ovular shapes as they shed vortices. Paired with this observation was an increase in drag coefficient as the compliant cylinder lengthened, and as the stiffness of their cylinder was increased at a Re of 400.

Higher drag forces imply that greater magnetic body forces would be required to maintain the aggregate as it lengthens, even neglecting the limited range of influence of the applied magnetic field. The change in drag coefficient found by Yokoyama and Mochizuki resulting from aspect ratio changes elucidate the significantly different aggregate decays at moderate Reynolds numbers between 400 and 700, where the final aggregate sizes diminish disproportionately between the fully stable cases and cases where shedding and aggregate washaway occurs. Yokoyama and Mochizuki additionally showed that not only do stiffer cylinders have higher drag coefficients, higher shedding frequencies are measured. As observed in Figure 12, our results are consistent with their findings for compliant cylinders, though the source of the stiffness change was from a magnetic field, rather than from the generalized mass-spring-damper system that they investigated. Figure 12 also shows relative aggregate lengthening as the Re is increased, and therefore, one can extrapolate that the aggregate is also subjected to higher drag coefficients as a result of the changing aspect ratio.

B. Aggregate decay scaling

Thus far, the temporal evolution of the aggregate under different flows and magnetic fields has been presented. However, the aggregate behavior can be more completely represented by distilling the time-series data into cumulative physical parameters. Therefore, we will now investigate the aggregate physics using the aggregate half-life, wall shear rate, and a dimensionless parameter developed for the ferrofluid-shear flow system.

First, we examine the half-lives of dispersing ferrofluid aggregates. For cases where at least a 50% drop in the aggregate size was recorded, the corresponding times are plotted as a function of the bulk flow Reynolds number in Figure 14. This data shows that elevated magnetic fields increase the rate of decay, resulting in faster washaway of the aggregate down to 50% size. This finding is complementary to Figure 12, which shows that the Strouhal number increases when the applied field is elevated. Generally, increasing the magnetic field results in aggregate stiffening due to increased magnetization of the aggregate, in the case where the aggregate is magnetized below the saturation magnetization value

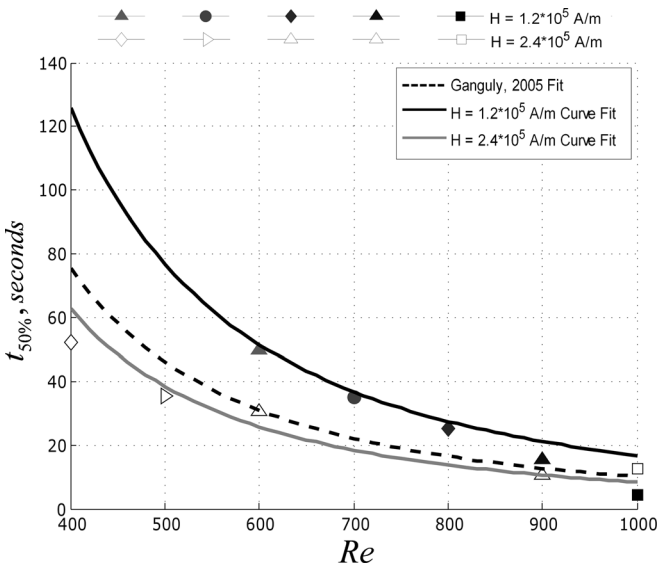

FIG. 14. Plot of the time to reach 50% of the original aggregate size as a function of the Reynolds number.

of the ferrofluid.[29] In this experiment, the aggregate magnetization is on the order of 10^{-5} Tesla at the aggregate interface, significantly below the saturation level of 0.022 Tesla. In a system containing a ferrofluid interacting in a shear flow, the magnetic forces oriented normal to the bulk flow can augment both the surface tension and body force effects associated with the development of the Kelvin-Helmholtz instability. This phenomenon is well documented, though largely through analytical studies.[9,30] Therefore, result of the increased magnetic field is faster aggregate dispersion, and lower half-life times. In addition, Figure 14 shows that the half life time is inversely dependent on the Reynolds number.

The Reynolds number dependence on half life in a ferrofluid system was also investigated by Ganguly *et al.*[22] Their experimental system examined ferrofluid accumulation and washaway an incident pulsatile flow with a 1 Hz frequency. They proposed an empirical power-law curve relating aggregate half-life ($t_{50\%}$, time at which the aggregate decays to half of its initial size) to the bulk flow Reynolds number by a power of −2.2. Figure 14 includes the power-law based fit of the projected half-life, as well as the half-life times determined for ferrofluid decay in this work. Symbols corresponding to data collected in the present experiment are plotted in contrast to the original curve fit from Ganguly *et al.*

It is apparent that the power law curve from Ganguly *et al.*, though a good fit for their dataset, does not capture the full range of ferrofluid aggregate dynamics. The discrepancy is expected, given that Ganguly *et al.* were examining a pulsatile flow, where ferrofluid was also accumulating at the magnet under an incident flow. Moreover, the curve from Ganguly *et al.* was generated from data where a single magnetic field strength and gradient were used, with an induction of 0.28 Tesla at the inner edge of the flow channel. However, the curve developed from their data remains relevant. Using the same exponent as the Ganguly curve fit, the predicted 50% time, scan be corrected so that it is representative of the

data collected in the present work by dividing a constant of 10^7 by the maximum value of the magnetic field at the inner edge of the flow channel each set of cases. This magnetic field is representative of differences in the peak body forces applied to the ferrofluid. The result of this correction is depicted in Eq. (4). The results of the curve fit are plotted in Figure 14 with dashed and solid lines for H_{max} of 2.4×10^5 and H_{max} of 1.2×10^5 A/m, respectively.

$$t_{50\%} = \frac{10^7}{B_{\max}} \mathrm{Re}^{-2.2} \tag{4}$$

After the time to decay to half of the original aggregate size, we will next consider the rate of change in aggregate size. The time-averaged rate of change of the aggregate as a function of the wall shear rate is shown in Figure 15. The rate of change was calculated using a second order, three point divided difference method, with the first 7 s of data neglected to remove transient effects. The wall shear rate was calculated as the flow rate, Q, divided by the cubed height of the channel, D_H. Building upon the relation of the half life to Reynolds number, a fourth order curve fit demonstrates that the decay of ferrofluid is non-linearly proportional to the wall shear rate, as observed by the varying temporal washaway of the aggregate. Cases with higher applied magnetic fields are plotted with open symbols while those with lower fields are shown with filled symbols.

The measured rate of dispersion versus wall shear rate can be compared with the 1993 work of Ruuge and Rusetski,[19] which is also plotted on Figure 15 as a dashed line. As extracted from the work of Ruuge and Rusetski, the decay rate is significantly lower than the decay rates from data obtained from this experiment. One source of this difference is the high value of F_M from Ruuge and Rusetski, of 10 600 dynes/cm^3. Conversely, the F_M corresponding to the present dispersion data are on the order of 1000–2000 dynes/cm^3 at the aggregate interface. Therefore, when comparing the two expected decay lines, the decay rate from Ruuge and Rusetski should be slower, as is the case in Figure 15 due to the higher magnetic body forces. An additional result from this analysis, intuitively, is that both the rate of decay and aggregate half lives are related to the applied magnetic field as well as incident flow. However, the nature of the average derivative is divergent between the data presented in Ruuge and Rusetski and the calculated aggregate derivatives measured herein.

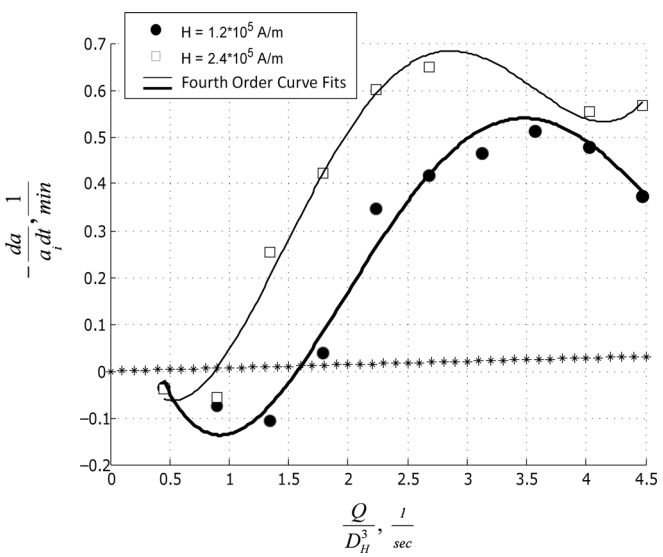

FIG. 15. The time-averaged change in aggregate size plotted versus wall shear rate. The solid linear curve fit developed from the data corresponding to the low (filled symbols) and high magnetic fields (open symbols). The dashed line corresponds to a fit of the rate of change versus wall shear rate measured in Ruuge and Rusetski.[19]

Given the difference in the decay rates between the two works, a comparison of the two sets of data from applied magnetic fields from the present work can be explored. It is probable that since the interfacial interaction changes significantly between the two magnetic fields presented herein, the regimes studied in this work may represent a transitional region for aggregate dynamics, particularly given the nonlinearity associated with the time-averaged derivative shown in Figure 15. As the magnetic fields are changed to higher or lower values, the aggregate would be expected to be either fully retained or immediately dispersed when exposed to an incident flow. As an additional distinction, Ruuge and Rusetski did not note any unsteady shedding behavior in their experiment, leading to the conclusion that washaway of their ferrofluid aggregates fell into a different regime. One explanation is associated with their selection of magnetic fluid, given that they examine saturation magnetization fluids a maximum of 1.4 gauss, whereas the EMG 705 fluid has a saturation magnetization of 220 gauss, which would provide significantly higher resistance to flow pressure. Moreover, the volume of injected ferrofluid in the work of Ruuge and Rusetski was between 0.05 to 0.3 ml within a 3 to 12 mm channel diameter. In the data presented herein, 2 ml of ferrofluid was injected for all cases within a 15 mm hydraulic diameter.

Following the half-life and decay rate, we will next discuss a parameter that synthesizes the major forces acting on the aggregate and capture its dynamics, expanding beyond these parameters. Based on the data collected, we infer that the dispersion process is governed by the interaction of the inertial and viscous forces and the balance between magnetic stresses and pressure on the aggregate-flow interface. Since the aggregate behaves as a compliant boundary, it creates a blockage, forcing localized flow acceleration. The presence of the magnetic field counters flow pressures, acting to retain the aggregate in the region of high field gradients. However, the interfacial dynamics between magnetic forces and flow shear creates an apparent "viscous" boundary that gives rise to instabilities, evolving into the Kelvin-Helmholtz shedding process. To further explore this interplay, the magnetic body force per specific volume was extracted at the half aggregate size, evaluated at the aggregate-bulk flow interface, using Eq. (3). A denominator that non-dimensionalizes the magnetic forces is given by

$$\overline{M} = \frac{\mu f_{shedding,50\%}}{h_{50\%}}, \tag{5}$$

where μ refers to the dynamic viscosity of water at ambient temperature, 0.01 poise. The parameter $f_{shedding,\ 50\%}$ is the shedding frequency measured at the time of 50% aggregate size, converted to radians per second, and finally, $h_{50\%}$ is the aggregate height at the 50% time in centimeters. Here, a distinction arises between the normalization shown in Figure 12 in that the non-dimensionalization is performed at the aggregate half-life. When studying the relative effects of the magnetic body forces and flow pressures, the half-life is the most representative means to account for the dynamic behavior of the aggregate. Using Eq. (5) to non-dimensionalize the magnetic forces results in the parameter F*

$$F = \frac{(M_{50\%} \bullet \nabla) H_{50\%}}{\overline{M}}. \tag{6}$$

The results of applying Eq. (6) are shown in Figure 16. Data from both magnetic fields is included, but is limited to cases with a defined half-life. Examining the parameters of Eq. (6) more closely, the values of $M_{50\%}$ increase relatively linearly as a function of Re. On the other hand, the denominator of F* increases as U^2 and is related to an unsteady flow pressure. Therefore, the physical extrapolation of F* is that even though the height of the aggregate is lower, in the cases of the higher Reynolds number, there is proportionally more aggregate shedding, even while the magnetic body forces are increasing. This competition between the parameters, captured in the F* equation, results in an overall decay curve which goes as the Reynolds number and is accurately described by an exponential curve fit with a linearized R^2 value of 0.98.

Each of the three parameters provides insight into the generalized mechanics of ferrofluid aggregates. The relative lengthening of the aggregate during increases of Re discussed in preceding paragraphs results in increased drag forces. The drag maintains aggregate shedding and also restricts the ability of the magnetic body forces to retain the aggregate, even as the aggregate height decreases. Though this work has expanded the body of knowledge related to ferrohydrodynamics, one limitation of this analysis is the reliance on a two-dimensional measurement of the aggregate, while the aggregate is subjected to three-dimensional effects. An additional limitation of this work is the assessment of the magnetic field effect based on datasets containing two magnetic fields. To fully generalize the non-dimensionalization, additional investigations must be undertaken. Despite these limitations, our results expand previous studies of ferrofluid aggregates. For the first time, we characterize the development of the Kelvin-Helmholtz instability by measuring the shedding frequency of the ferrofluid. Also, the half life time model proposed by Ganguly *et al*. has been extended and corrected to account for a larger span of flows as well as different magnetic fields. Finally, the parameter F* has been developed accounting for the influence of flow and magnetic fields.

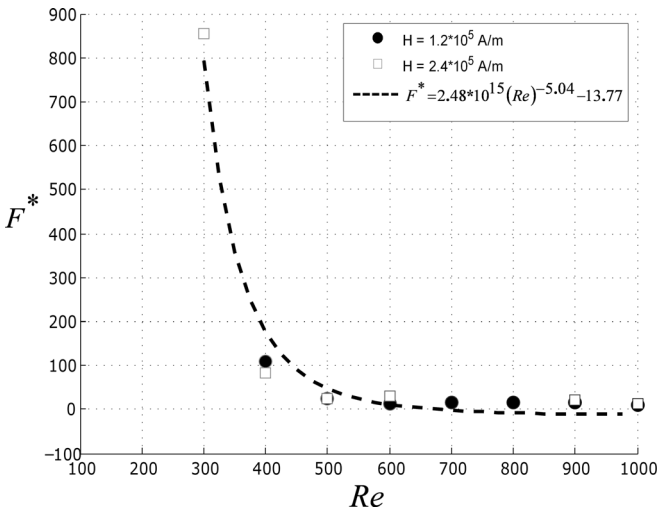

FIG. 16. Plot of the normalized magnetic body force per unit volume versus the Reynolds number. The results of a power law curve fit are shown using the black dashed line.

IV. CONCLUSIONS

The behavior of ferrofluid aggregates was studied herein for steady flow conditions over a range of Reynolds numbers spanning 100 to 1000. Three regimes apparent for flows of Re between 100 and 1000 were identified based on maximum magnetic fields of 2×10^5 and 2.4×10^5 A/m. Reynolds numbers less than 300 for both fields result in a stable aggregate that stretches in the x and y-directions by up to 8%. At the transitional Reynolds numbers, the aggregate stretches significantly, losing coherence as it shears away from high magnetic field gradients. Ferrofluid stretching leads to interfacial ripples and light ferrofluid tendrils shed periodically downstream. Further increase of the Reynolds number results in Kelvin-Helmholtz shedding from the main aggregate and aggregate erosion of up to 80 percent over 60 s.

Generally, the temporally sampled Strouhal number increases with Reynolds number, since the increased Re drives increases in shedding frequency. The influence of different magnetic fields results in aggregate shedding initiation at a lower Reynolds number as well as an increase in the shedding frequency for a given Reynolds number in the shedding regime. The aggregate half life, decay rate, and a newly developed dimensionless body force parameter are used to holistically elucidate aggregate dynamics. The aggregate half life decreases proportionally to $Re^{-2.2}$, multiplied by an additional correction factor to account for magnetic body forces. In addition, the decay rate of ferrofluid is proportional to the wall shear rate. Finally, a dimensionless parameter containing the specific volume-based magnetic body force, along with the aggregate height and shedding frequency, calculated at the aggregate half-life captures the data effectively. A resulting empirical fit is proportional to $Re^{-5.3}$, indicating a power law decay relationship between the interaction of aggregate-directed forces and the bulk flow.

[1]J. C. Bacri, R. Perzynski, M. I. Shliomis, and G. I. Burde, ""Negative-viscosity" effect in a magnetic fluid," Phys. Rev. Lett. **75**, 2128 (1995).
[2]M. I. Shliomis, "Comment on "Structure of ferrofluid dynamics,"" Phys. Rev. E **67**, 043201 (2003).
[3]B. Abou, J. E. Wesfreid, and S. Roux, "The normal field instability in ferrofluids: Hexagon-square transition mechanism and wavenumber selection," J. Fluid Mech. **416**, 217 (2000).
[4]A. G. Boudouvis, J. L. Puchalla, L. E. Scriven, and R. E. Rosensweig, "Normal field instability and patterns in pools of ferrofluid," J. Magn. Magn. Mater. **65**, 307 (1987).

[5]M. Zahn and R. Rosensweig, "Stability of magnetic fluid penetration through a porous medium with uniform magnetic field oblique to the interface," IEEE Trans. Magn. **16**, 275 (1980).
[6]G. Pacitto, C. Flament, J. C. Bacri, and M. Widom, "Rayleigh-Taylor instability with magnetic fluids: Experiment and theory," Phys. Rev. E **62**, 7941 (2000).
[7]S. K. Malik and M. Singh, "Finite amplitude Kelvin–Helmholtz instability in magnetic fluids," Phys. Fluids **29**, 2853 (1986).
[8]G. Moatimid, "Nonlinear Kelvin-Helmholtz instability of two miscible ferrofluids in porous media," ZAMP **57**, 133 (2005).
[9]J. A. Miranda and M. Widom, "Parallel flow in Hele-Shaw cells with ferrofluids," Phys. Rev. E **61**, 2114 (2000).
[10]K. Raj and R. Moskowitz, "Commercial applications of ferrofluids," J. Magn. Magn. Mater. **85**, 233 (1990).
[11]C. Alexiou, W. Arnold, P. Hulin, R. J. Klein, H. Renz, F. G. Parak, C. Bergemann, and A. S. Lubbe, "Magnetic mitoxantrone nanoparticle detection by histology, x-ray and MRI after magnetic tumor targeting," J. Magn. Magn. Mater. **225**, 187 (2001).
[12]C. Alexiou, W. Arnold, R. J. Klein, F. G. Parak, P. Hulin, C. Bergemann, W. Erhardt, S. Wagenpfeil, and A. S. Lubbe, "Locoregional cancer treatment with magnetic drug targeting," Cancer Res. **60**, 6641 (2000).
[13]C. Alexiou, R. Jurgons, R. Schmid, A. Hilpert, C. Bergemann, F. Parak, and H. Iro, "*in vitro* and *in vivo* investigations of targeted chemotherapy with magnetic nanoparticles," J. Magn. Magn. Mater. **293**, 389 (2005).
[14]C. Alexiou, R. Jurgons, R. J. Schmid, C. Bergemann, J. Henke, W. Erhardt, E. Huenges, and F. Parak, "Magnetic drug targeting–biodistribution of the magnetic carrier and the chemotherapeutic agent mitoxantrone after locoregional cancer treatment," J. Drug Target. **11**, 139 (2003).
[15]C. Alexiou, A. Schmidt, R. Klein, P. Hulin, C. Bergemann, and W. Arnold, "Magnetic drug targeting: Biodistribution and dependency on magnetic field strength," J. Magn. Magn. Mater. **252**, 363 (2002).
[16]A. S. Lubbe, C. Alexiou, and C. Bergemann, "Clinical applications of magnetic drug targeting," J. Surg. Res. **95**, 200 (2001).
[17]A. S. Lubbe, C. Bergemann, H. Riess, F. Schriever, P. Reichardt, K. Possinger, M. Matthias, B. Dorken, F. Herrmann, R. Gurtler, P. Hohenberger, N. Haas, R. Sohr, B. Sander, A.-J. Lemke, D. Ohlendorf, W. Huhnt, and D. Huhn, "Clinical experiences with magnetic drug targeting: A phase I study with 4'-epidoxorubicin in 14 patients with advanced solid tumors," Cancer Res. **56**, 4686 (1996).
[18]A. N. Rusetski and E. K. Ruuge, "Magnetic fluid as a possible drug carrier for thrombosis treatment," J. Magn. Magn. Mater. **85**, 299 (1990).
[19]E. K. Ruuge and A. N. Rusetski, "Magnetic fluids as drug carriers: Targeted transport of drugs by a magnetic field," J. Magn. Magn. Mater. **122**, 335 (1993).
[20]R. Ganguly, A. P. Gaind, S. Sen, and I. K. Puri, "Analyzing ferrofluid transport for magnetic drug targeting," J. Magn. Magn. Mater. **289**, 331 (2005).
[21]R. Ganguly and I. K. Puri, in *Advances in Applied Mechanics*, edited by H. A. a. E. v. d. Giessen (Elsevier, Orlando, Florida, 2007), Vol. 41.
[22]R. Ganguly, B. Zellmer, and I. K. Puri, "Field-induced self-assembled ferrofluid aggregation in pulsatile flow," Phys. Fluids **17**, 097104 (2005).
[23]N. Otsu, "Threshold selection method from grayscale histograms," IEEE Trans. Syst. Man Cybern. **9**, 62 (1979).
[24]V. Madisetti and D. B. Williams, *The Digital Signal Processing Handbook* (CRC, New York, 1998).
[25]S. L. Jae and V. O. Alan eds, *Advanced Topics in Signal Processing* (Prentice-Hall, Inc., Englewood Cliffs, NJ, 1987).
[26]A. Roshko, "Experiments on the flow past a circular cylinder at very high Reynolds number," J. Fluid Mech. **10**, 345 (1961).
[27]C. H. K. Williamson, "Oblique and parallel modes of vortex shedding in the wake of a circular cylinder at low reynolds numbers," J. Fluid Mech. **206**, 579 (1989).
[28]M. Yokoyama and O. Mochizuki, "Deformation of a fluid-filled compliant cylinder in a uniform flow," J. Fluids Struct. **25**, 1049 (2009).
[29]T. Weser and K. Stierstadt, "Magnetoviscosity of concentrated ferrofluids," Z. Phys. B **59**, 257 (1985).
[30]R. E. Rosensweig, *Ferrohydrodynamics* (Cambridge University Press, New York, 1985), republished by Dover, 1997.